Intergranular films at Au-sapphire interfaces

Mor Baram · Wayne D. Kaplan

Abstract The existence of nanometer-thick amorphous equilibrium films at metal-ceramic interfaces has been experimentally verified for the Au–Al_2O_3 system. The films were formed using a novel experimental approach, in which thin sputtered films of Au were dewetted on a sapphire substrate which was previously partially wetted with drops of anorthite glass (CaO–$2SiO_2$–Al_2O_3). High-resolution transmission electron microscopy and qualitative analytical transmission electron microscopy were used to confirm the existence of the amorphous films. In addition, positive and relatively large Hamaker constants were calculated for the Au-film-Al_2O_3 interface, which indicates the existence of an attractive van der Waals force which stabilizes the film, similar to equilibrium films at grain boundaries in ceramics. A ~ 1 nm thick surface film was also detected on the (0001) surface of sapphire substrates partially wetted by anorthite glass. The refractive index required to stabilize the surface films, via a positive Hamaker constant, is explored.

Introduction

Over three decades ago the first equilibrium intergranular films (IGFs) were found and characterized at grain boundaries in polycrystalline Si_3N_4 [1–3]. Since then

M. Baram · W. D. Kaplan (✉)
Department of Materials Engineering, Technion–Israel
Institute of Technology, Haifa 32000, Israel
e-mail: kaplan@tx.technion.ac.il

IGFs were observed at grain boundaries in several other polycrystalline ceramic systems, including SiC [4–9], Al_2O_3 [10–12], thick-film resistors [13] and varistors [14–15]. Luo et al. found stable disordered films at oxide surfaces [15, 16]. In addition, extensive structural, chemical and theoretical analysis of IGFs in the Si_3N_4 system has been conducted [17–28]. The existence of IGFs in these systems results mainly from impurities and/or sintering aids which lead to the formation of bulk liquid phases in the polycrystalline ceramic microstructure.

In contrast to IGFs in ceramic systems, thin equilibrium films at metal-ceramic interfaces were only recently found and investigated [29–32]. Scheu et al. showed the existence of IGFs in Cu–Al_2O_3 composites prepared by melt-infiltration, apparently due to the presence of impurities in the initial Al_2O_3 powders [29]. Avishai et al. gave further validation to the existence of IGFs at Cu–Al_2O_3 interfaces, as well as at Ni–Al_2O_3 interfaces, via detailed microstructural investigations of interfaces in model metal-particle reinforced polycrystalline alumina composites, which included defined amounts of glass forming additives [30].

IGFs have a uniform thickness of the order of ~1 nm in all the systems specified above [1–5, 7–20, 23, 29, 30]. In several systems this thickness has been shown to depend on the specific composition of the film [12, 18]. The film thickness as a function of orientation of the boundary defining grains is ambiguous. At grain boundaries in silicon nitride no such dependence was found [33], while the thickness of films at interfaces between dissimilar materials has been shown to depend on the orientation of the interface-defining crystals [29, 34]. Extensive analytical measurements conducted on

the films in alumina-based systems have shown that they are mainly based on Ca, Si, and Al, and other elements originating from impurities in the initial materials [1–5, 7–20, 23, 29, 30]. In some cases the composition of the intergranular phase was close to that of anorthite (CaO–2SiO$_2$–Al$_2$O$_3$) in the SiO$_2$–Al$_2$O$_3$–CaO ternary system [10, 30, 35].

One of the reasons for the interest in IGFs comes from their influence on macroscopic properties. IGFs in ceramic-ceramic structural materials can significantly influence mechanical properties [35], by degrading high-temperature strength [36] on one hand and enhancing fracture toughness, strength and fatigue properties on the other hand [37–43]. In thick-film resistors, the existence of IGFs was found to influence the electrical properties [13]. The influence of IGFs on properties in metal-ceramic systems has not been widely studied, although they have been shown to reduce the fracture toughness of diffusion bonded Pt–Al$_2$O$_3$ interfaces [44].

The formation and existence of IGFs have been explained over the years by different theories, in terms of multi-layer adsorption and prewetting films [45–47]. In addition, the stability and equilibrium thickness of thin amorphous films was considered by Clarke et al. in a force-balance model [48, 49]. They showed that for a stable film thickness to exist there should be a force balance between attractive forces (e.g. van der Waals forces) and repulsive forces (e.g. steric interactions originating from partial ordering of the nominally amorphous film). Avishai et al. applied Clarke's approach to the case of an amorphous film at metal-ceramic interfaces, and showed a positive and relatively large Hamaker constant for amorphous films based on Si and Ca at Cu–Al$_2$O$_3$ and Ni–Al$_2$O$_3$ interfaces [32].

Most studies of IGFs have focused on polycrystalline systems, which include glass-forming additives and are allowed to equilibrate at high temperature. In the present study a different experimental approach is evaluated, where sub-micron liquid Au drops are equilibrated in contact with the basal (0001) surface of sapphire in the presence of anorthite glass. We show that equilibrium IGFs also exist at Au–Al$_2$O$_3$ interfaces formed by this process.

Experimental methods

Wetting and dewetting experiments

Basal plane (0001) oriented sapphire (α-Al$_2$O$_3$) substrates of 99.99% purity were provided by Gavish Industrial Technologies & Materials. Prior to wetting and dewetting experiments, the substrates were ultrasonically cleaned in acetone and ethanol, and thermally annealed for 2 h at 1200 °C in air.

Anorthite (CaO–2SiO$_2$–Al$_2$O$_3$) was prepared by ultrasonic mixing of 34 g of Al$_2$O$_3$ powder (Sumitomo AKP 50) with 30.03 g of CaCO$_3$ and 36.05 g SiO$_2$ in 25 g H$_2$O. The paste was dried and then heat treated in air at a temperature of 1600 °C for 4 h to obtain anorthite glass. After equilibration, the anorthite glass was ground to a fine powder, mixed into a slurry using ethanol and dispersed on the surface of the sapphire substrates. After drying, the coated sapphire substrates were heat treated at 1600 °C for 1 h to form micron-sized droplets of glass on the (0001) sapphire surfaces. Another set of samples was prepared using the same procedure, but bulk pieces of anorthite glass were partially wetted on the annealed sapphire substrate. In the following, identical results were obtained regardless of the method used to wet the sapphire substrates with anorthite.

At this stage a ~60 nm thick Au film was deposited on the substrates using a Polaron sputter coater. The specimens were annealed in air at 1100 °C for 5 min. Since at this temperature Au is in a liquid state (Tm = 1064 °C), dewetting of the Au film will occur due to the finite contact angle of Au on sapphire [50]. This resulted in an extremely large number of sub-micron sized Au droplets on the sapphire substrates as well as on the anorthite drops, as described in the schematic drawing shown in Fig. 1.

Characterization methods

The morphology of the anorthite and Au drops was characterized using high resolution scanning electron microscopy (HRSEM). HRSEM was conducted on a LEO 982 Gemini microscope equipped with a field emission gun (FEG–SEM). A dual-beam focused ion beam (FIB) (FEI Strata 400-S) equipped with a high angle annular dark field (HAADF) scanning transmission electron microscopy (STEM) detector and nano-manipulator (Omniprobe, AutoProbe 200) was used to prepare cross-section TEM specimens from the center of Au particles using the "lift out" technique [51]. Low incident angle and low voltage (2 kV) FIB milling was
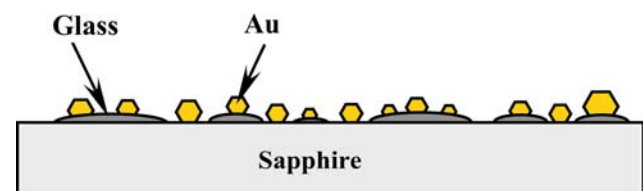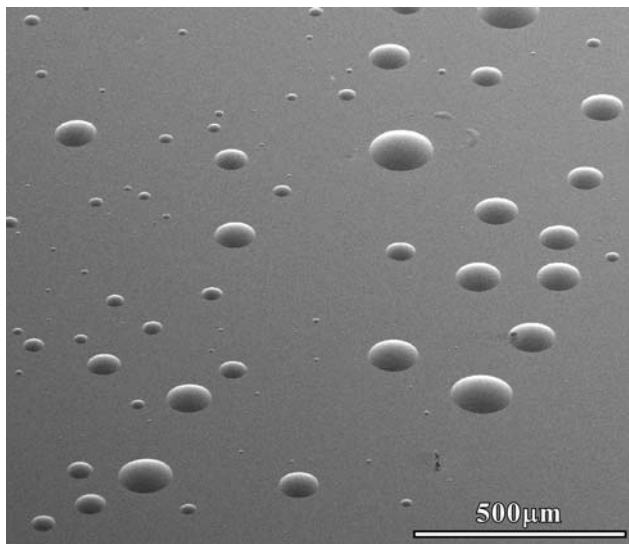

Fig. 1 Schematic drawing of the samples prepared by the dewetting process

conducted at the end of the TEM specimen preparation process to reduce the thickness of the surface layers damaged by the FIB milling process [52]. The morphology of the Au–Al$_2$O$_3$ interfaces was characterized using transmission electron microscopy (TEM), conducted on three different microscopes. The first was a JEOL 3010UHR microscope, operated at 300 kV and with a point resolution better than 0.16 nm. The second was a FEI Tecnai F20 G^2 FEG microscope operated at 200 kV with a point resolution better than 0.24 nm, equipped with a HAADF STEM detector, an energy dispersive X-ray spectrometer (EDS) and energy filtered TEM–EFTEM (GATAN Imaging Filter 2001). In addition, a FEI Titan 80–300 kV FEG-TEM with an aberration corrector was used to characterize the interface structure.
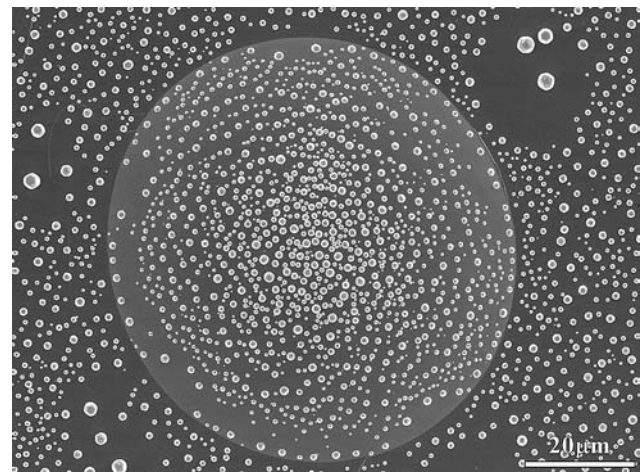
Results and discussion

Surface morphology after dewettting

Figure 2 presents a secondary electron SEM micrograph of a sapphire substrate after (partial) wetting with anorthite drops. Examination of the specimens after the Au dewetting process revealed that the gold particles were located on the (apparently) glass-free sapphire substrate as well as on the anorthite drops (see Fig. 3). Next to the large (~60 μm) anorthite drop visible in Fig. 3, areas with coarsened Au particles are evident. Numerous gold particles were found on the

Fig. 3 Secondary electron SEM micrograph of a (0001) sapphire substrate after partial wetting with anorthite and dewetting of the Au film. The Au particles are located on both the large anorthite drop (~60 μm) and the (apparently) glass-free sapphire substrate

anorthite drops, which were a few microns in diameter. If the anorthite drop was small enough, only one gold particle was found on the center of the drop (see Fig. 4). The faceted shape of the Au particles follows the equilibrium shape of solid Au in air [53]. In addition, grain boundary grooves are visible in some of the particles, indicating that they are not single crystalline particles. Immediately adjacent to the Au particles the sapphire surface is not flat. From SEM alone it is not clear whether this is due to the presence
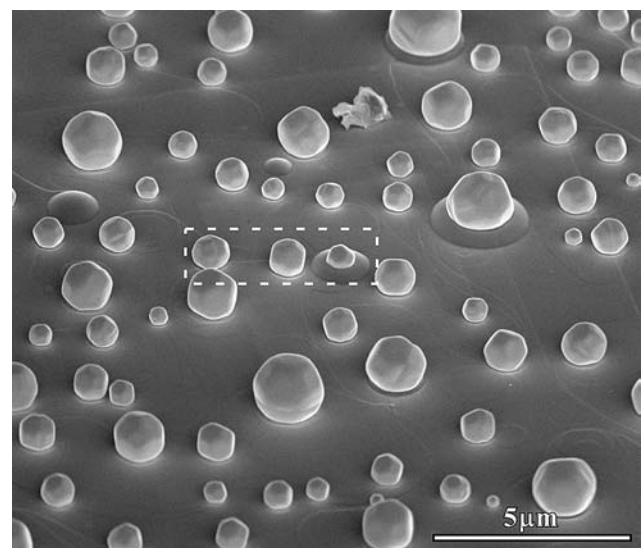

Fig. 2 Secondary electron SEM micrograph of a (0001) sapphire substrate after partial wetting with anorthite. This specimen was coated with a thin film of Ni to prevent charging during SEM investigations

Fig. 4 Secondary electron SEM micrograph (acquired using the dual-beam FIB) showing a single Au particle that "sank" inside an anorthite drop. The Au particles are facetted, and some of the particles contain grain boundaries. TEM specimens were prepared from the three drops indicated by the dashed white line
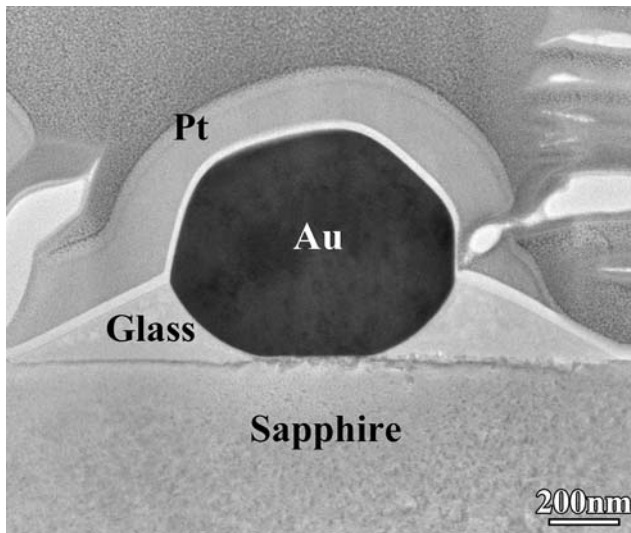
Fig. 5 Bright field TEM micrograph of an Au particle which "sank" in an anorthite drop. This specimen was prepared using the FIB "lift out" technique. The contrast above the gold is from the protective Pt coating that was deposited prior to the FIB "lift-out" process

of glass films, facets [54–56], or curvature changes at the sapphire-Au-air triple junctions, which is exposed upon contraction of the Au particles during solidification [57–59]. As discussed in the following sections, TEM studies show that curvature changes at the triple junctions do not occur, and surface films do exist adjacent to the glass drops.

Intergranular films at the Au-sapphire interface

Cross-section TEM specimens were prepared from the Au particles located on small anorthite drops and from Au particles on the sapphire *adjacent* to anorthite drops, as presented in Fig. 4. Figure 5 presents a bright field TEM micrograph of a gold particle, which "sank" inside the anorthite drop. The sinking of the Au particle

in the anorthite drop can be explained by the relatively high specific density of gold compared to anorthite, and the relatively low viscosity of the glass at the annealing temperature. The Au-sapphire interfaces were examined by HRTEM and an IGF was detected at the interface for the Au particle, which "sank" through the glass (see Fig. 6), and for the Au particle adjacent to the glass drop (see Fig. 7). The thickness of the intergranular film was constant along the entire interface.

An interesting phenomenon occurred during TEM examination of the bulk glass. The glass partially crystallized under the electron beam at high magnifications in a matter of seconds, as can be seen in the Fig. 6. This was not detected during previous TEM studies of IGFs at metal-ceramic interfaces [30], and may be due to the fact that the TEM specimens in this study were prepared by FIB milling [52].

Thickness measurements

The thickness of the films was measured from several micrographs, for each of the two different cases (particles which "sank" through the glass drop and particles located adjacent to an anorthite drop). The thickness was measured from intensity line-scans measured perpendicular to the interface, and averaged over entire micrographs (~20 nm's parallel to the interface). The results are presented in Table 1. The data presented here is from micrographs acquired after small electron doses, to minimize the electron irradiation damage. The values in Table 1 are ~1 nm, which agree well with previous thickness measurements of intergranular films at metal-ceramic interfaces [29, 30, 32].

Qualitative and quantitative chemical analysis

EDS analysis of the glass drops in which the Au particle "sank" was conducted. An EDS spectrum as
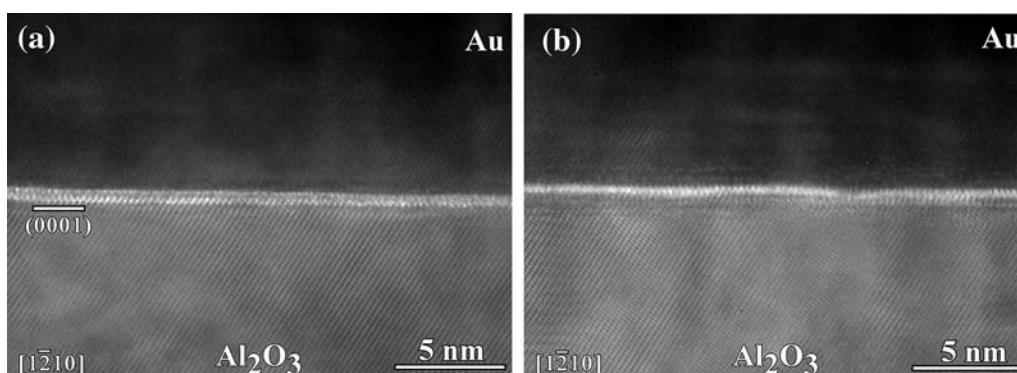
Fig. 6 HRTEM micrographs of the intergranular film at the interface of a Au particle which "sank" through the glass drop, (a) after a relatively short exposure to the 300 kV TEM electron beam, and (b) after several minutes of exposure to the electron beam
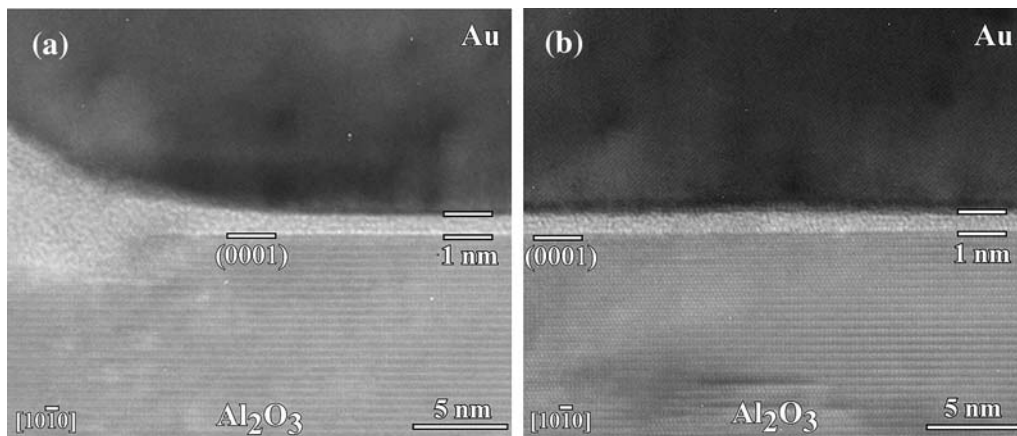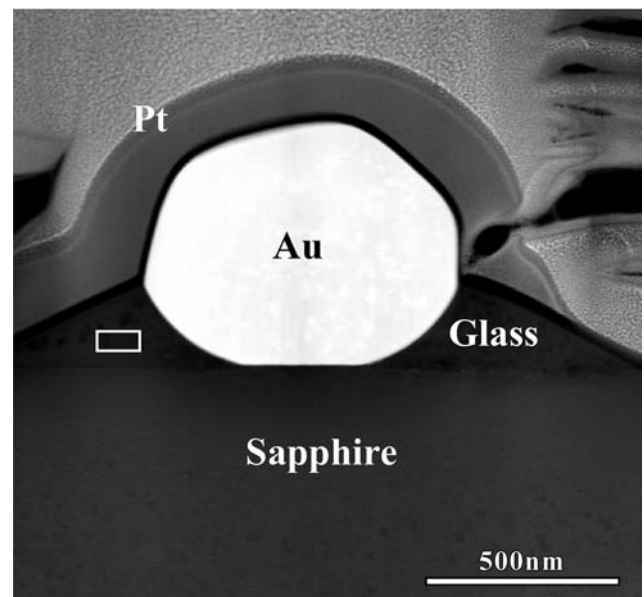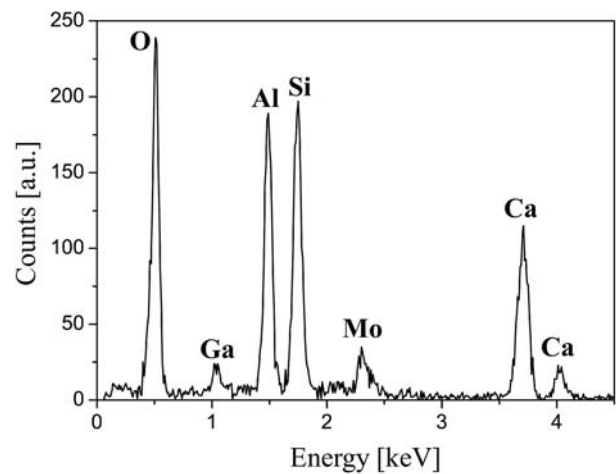
Fig. 7 HRTEM micrographs of an intergranular film at an Au–Al$_2$O$_3$ interface from an Au particle located adjacent to a glass drop: (a) from the triple junction region; (b) from the center of the Au particle

well as a STEM image indicating the location from which the measurement was acquired are presented in Fig. 8. The quantified chemical analysis from the EDS analysis is presented in Table 2.

The values in Table 2 validate that the glass is indeed anorthite, and that the composition is relatively constant within the volume of the triple-junction. Y contamination was found in only one of the samples, and is due to contamination introduced during grinding of the anorthite powder.

In addition to validation of the existence of the film from HRTEM, analytical microscopy was conducted to determine the major elements in the film. Initially, EDS line-scans were conducted across the interface (see Fig. 9). A statistically significant increase in Ca and Si counts are detectable at the interface. To give further confirmation to the EDS line-scan results, an EFTEM elemental map of Ca was obtained from the triple-junction region (see Fig. 10). A thin white line can be observed at the interface, which confirms the existence of Ca in the IGF.
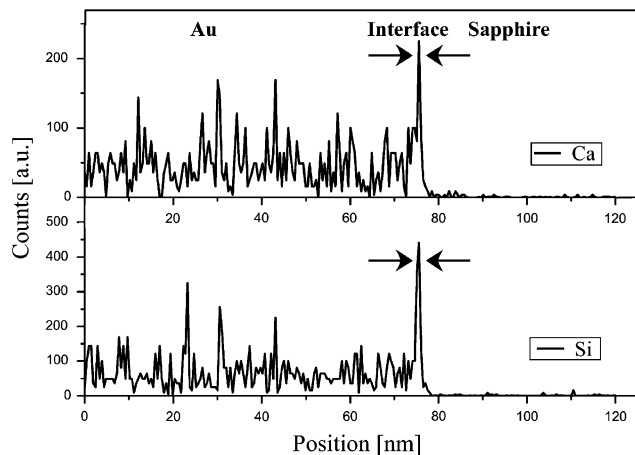

Table 1 Film thickness measurements determined from HRTEM micrographs, from both types of particles (two particles from each type). In a manner similar to previous studies [31], the influence of delocalization on the error of the thickness measurements was ignored [60]

| Type of Particle	Film Thickness [nm]	
Particle which "sank" through the glass drop	1.01 ± 0.04	
Particle adjacent to a glass drop*	0.94 ± 0.07	0.76 ± 0.07

*The two different values represent films measured from two Au–Al$_2$O$_3$ interfaces which are at different distances from the anorthite drops (see Fig. 13)

Fig. 8 (a) EDS spectrum acquired from an anorthite glass drop; and (b) STEM micrograph presenting the area from which the EDS measurement was performed

Table 2 EDS results measured from anorthite drops in which Au particles "sank". The results were acquired from three locations in two cross-section TEM specimens

Element	Concentration [at.%]			
	Location 1 Sample 1	Location 2 Sample 1	Location 3 Sample 2	Theoretical values for anorthite
O	57.5	60.4	49.7	58.3
Al	15.4	15.3	19.6	16.6
Si	17.9	16.9	20.3	16.6
Ca	6.7	5.1	10.5	8.3
Y	2.3	2.3	–	–
Na	0.5	–	–	–

Fig. 9 EDS line-scan acquired perpendicular to the Au-sapphire interface showing the presence of Si and Ca at the interface
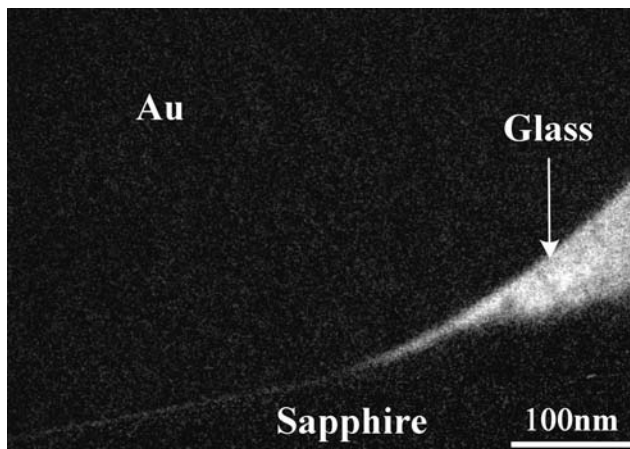
Fig. 10 EFTEM elemental map of Ca acquired from the triple junction region between a Au particle which "sank" through a glass drop to the interface with the sapphire substrate
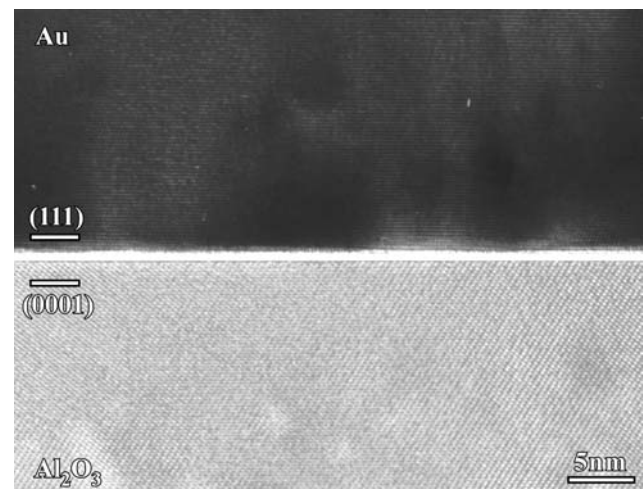
"Dry" Au-sapphire interface

To exclude possibilities that TEM artifacts or substrate contamination are responsible for the contrast at the Au-sapphire interfaces, a comparison was made to an Au-sapphire interface equilibrated without the presence of anorthite. This specimen was annealed at 1100 °C for 0.5 h and then cooled to 1000 °C and annealed for 100 h in air, followed by rapid cooling to room temperature [53]. An IGF was not detected at this interface, although it was equilibrated (under the same furnace conditions) for far longer than the specimens dewetted in the presence of anorthite (see Fig. 11). It is important to note that this TEM specimen was also prepared by the FIB "lift out" technique, which rules out the sample preparation process as being responsible for the presence of the amorphous film at Au-sapphire interfaces for samples prepared in the presence of anorthite. The bright contrast at the interface might be due to a degree of interface segregation [31] or contrast delocalization [60], but an amorphous film is not detected.

Surface films

An obvious question is whether a surface film (on the sapphire) was created *after* partial wetting with anorthite and *prior* to dewetting with gold. In order to address this question, a cross-section TEM specimen was prepared immediately after wetting the sapphire substrate with anorthite. In order to protect the free


Fig. 11 HRTEM micrograph of a Au-sapphire interface equilibrated without the presence of anorthite

surface during the TEM specimen preparation process, the sample was coated with ~200 nm of Ni prior to TEM specimen preparation. A TEM specimen was prepared from a region immediately adjacent to an anorthite drop, using the FIB "lift out" technique. Figure 12 presents a HRTEM micrograph from this sample, which clearly shows the presence of a ~0.9 nm thick amorphous film on the sapphire surface.

The thickness of the intergranular and surface films as a function of distance from the anorthite drops was also examined. In Fig. 13, the thickness of the film at four different distances is presented. The first three results are from films at Au-sapphire interfaces, while the fourth is from the surface film. It is interesting to note that for films at the Au-sapphire interface, the
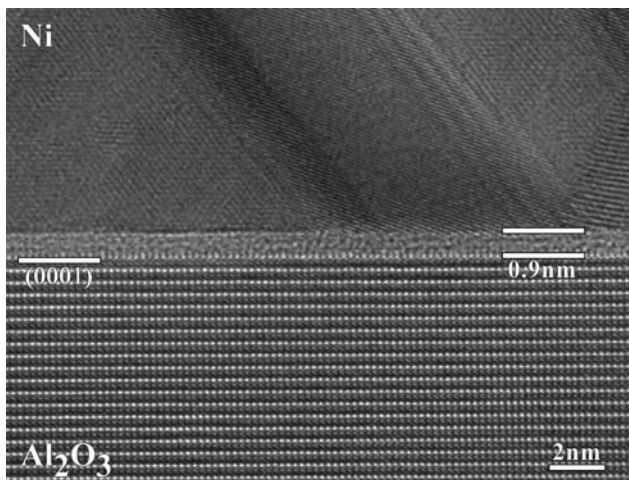
Fig. 12 HRTEM micrograph of the (0001) sapphire surface after partial wetting with anorthite. The micrograph was acquired from a region of the surface adjacent to a glass drop. Prior to specimen preparation, the sample was coated with a ~200 nm thick Ni film
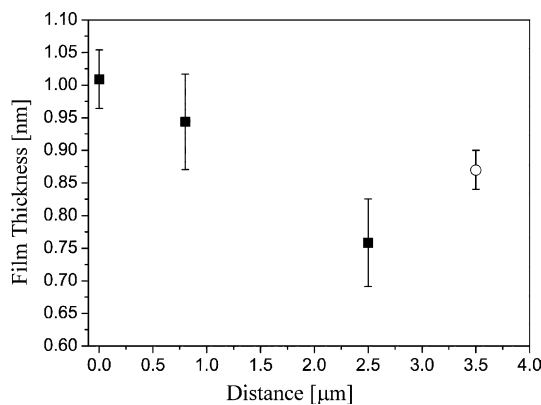
Fig. 13 Intergranular film thickness as a function of distance from the anorthite drop. (■) are values measured from Au–Al$_2$O$_3$ interfaces, and (○) was measured from the surface film

film is *thinner* as the distance from the anorthite drop increases. However, the thickness of the surface film has an intermediate value, while it was measured further away (3.5 μm) from an anorthite drop. This may indicate that the chemical composition of the films (as a function of distance from the anorthite drops) has not equilibrated. The thickness of the film is expected to depend on its refractive index (and thus its composition). This issue is addressed via calculation of the Hamaker constants for surface films in the following section.

Hamaker calculations

The Hamaker constant for the case of two solids interacting through a third medium can be expressed by:

$$H_{\alpha\beta\gamma} \approx \frac{3}{4}kT\left(\frac{\varepsilon_{\alpha(0)} - \varepsilon_{\beta(0)}}{\varepsilon_{\alpha(0)} + \varepsilon_{\beta(0)}}\right)\left(\frac{\varepsilon_{\gamma(0)} - \varepsilon_{\beta(0)}}{\varepsilon_{\gamma(0)} + \varepsilon_{\beta(0)}}\right)$$
$$+ \frac{3\hbar}{2}\int_{v_1}^{\infty}\left(\frac{\varepsilon_{\alpha(iv)} - \varepsilon_{\beta(iv)}}{\varepsilon_{\alpha(iv)} + \varepsilon_{\beta(iv)}}\right)\left(\frac{\varepsilon_{\gamma(iv)} - \varepsilon_{\beta(iv)}}{\varepsilon_{\gamma(iv)} + \varepsilon_{\beta(iv)}}\right)dv \quad (1)$$

where $\varepsilon_{(iv)}$ is the frequency-dependent dielectric constant for the different (α, β, γ) phases, v is the frequency, k is Boltzmann's constant, T is the absolute temperature, and $\hbar$ is Plank's constant divided by 2π. The frequency dependent term is integrated from the thermal frequency v_1 to infinity (above 100 eV the contribution is negligible) [32]. The first term is the zero frequency term, which consists of the Debye and Keesom contribution to the van der Waals force, while the second term is the frequency dependent term, which represents the London dispersion interactions.

By using the Ninham-Parsegian representation the dielectric properties of the materials can be obtained, since these values are not readily available for most materials. The frequency dependent dielectric constant of the ceramic material can be calculated from [32]:

$$\varepsilon_{\text{ceramic}(iv)} = 1 + \frac{\varepsilon_{\text{ceramic}(0)} - n_{\text{ceramic}}^2}{1 + v/v_{\text{rot,ceramic}}}$$
$$+ \frac{n_{\text{ceramic}}^2 - 1}{1 + \left(v/v_{\text{e,ceramic}}\right)^2} \quad (2)$$

where n_{ceramic} is the refractive index, and $v_{\text{rot,ceramic}}$ and $v_{\text{e,ceramic}}$ are the absorption frequencies in the IR and UV, respectively. $v_{\text{rot,ceramic}}$ can be neglected since integration is from the thermal frequency (~4·10^{-13} s^{-1}) and for most materials the rotational frequency is lower [32]:

$$\varepsilon_{\text{ceramic}(i\upsilon)} = 1 + \frac{n_{\text{ceramic}}^2 - 1}{1 + \left(\upsilon/\upsilon_{\text{e,ceramic}}\right)^2} \qquad (3)$$

For the metal, the frequency dependent dielectric permittivity can be calculated from [32]:

$$\varepsilon_{\text{metal}(i\upsilon)} = 1 + \left(\frac{\upsilon_{\text{e,metal}}}{\upsilon}\right)^2 \qquad (4)$$
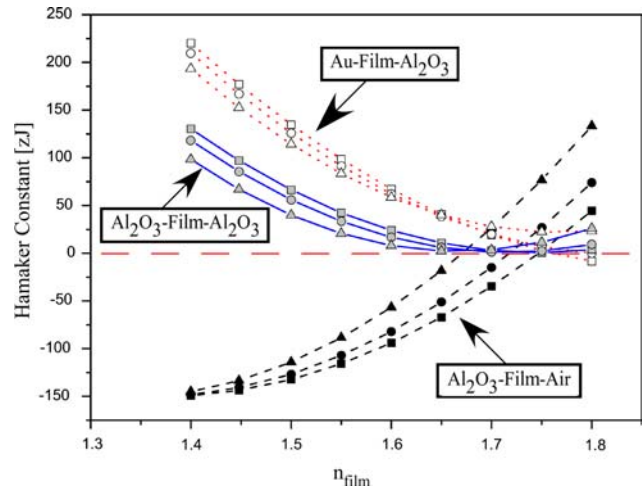
where $\upsilon_{\text{e,metal}}$ is the plasmon frequency.

The static dielectric constant of a metal is infinite, so for metal-ceramic interfaces the Hamaker constant may be obtained from (α-ceramic, β-film, γ-metal):

$$H_{\alpha\beta\gamma} \approx \frac{3}{4}kT\left(\frac{\varepsilon_{\alpha(0)} - \varepsilon_{\beta(0)}}{\varepsilon_{\alpha(0)} + \varepsilon_{\beta(0)}}\right)$$
$$+ \frac{3\hbar}{2}\int_{\upsilon_1}^{\infty}\left(\frac{\varepsilon_{\alpha(i\upsilon)} - \varepsilon_{\beta(i\upsilon)}}{\varepsilon_{\alpha(i\upsilon)} + \varepsilon_{\beta(i\upsilon)}}\right)\left(\frac{\varepsilon_{\gamma(i\upsilon)} - \varepsilon_{\beta(i\upsilon)}}{\varepsilon_{\gamma(i\upsilon)} + \varepsilon_{\beta(i\upsilon)}}\right)d\upsilon \qquad (5)$$

The Hamaker constants for a Au-film-Al₂O₃ interface, a grain boundary in Al₂O₃ containing an IGF, and a surface film on sapphire were calculated (Matlab Ver. 7.0) using the data of Al₂O₃, SiO₂ and Au as presented in Table 3. Since there is a lack of necessary data to estimate the Hamaker constant for an interface containing an anorthite-based film, the calculations were first made for a SiO₂-based film. The influence of Ca and Al additions in the SiO₂ film on the refractive index and UV absorption frequency, and in turn on the Hamaker constant, were examined following the approach used by Avishai and Kaplan [32], and are presented in Fig. 14. The range of values was selected because the optical properties of the film (and its exact composition) are not known. The range of refractive indices chosen was based on the refractive indices of different compositions in the SiO₂–Al₂O₃–CaO ternary system as presented in Table 4. The values of UV absorption frequencies were selected based on previous studies. The UV absorption frequency of anorthite (and the film) may be lower than the values used here [32], which means that the calculated value of the Hamaker constant will be lower (see Fig. 14). The

Fig. 14 Calculated Hamaker constants versus refractive index and UV absorption frequency for metal-alumina interfaces, a grain boundary in alumina, and a surface film on alumina. ($\square$) is for a UV absorption frequency of $3.24\cdot10^{15}$ Hz, ($\bigcirc$) is for a UV absorption frequency of $3.5\cdot10^{15}$ Hz and (Δ) is for a UV absorption frequency of $4\cdot10^{15}$ Hz

influence of the zero frequency term and the temperature were also examined, but found to be negligible.

There are several points that should be noted from the results of the calculations. First, the Hamaker constant for an Au-sapphire interface containing a film is indeed positive, and following Clarke's model, can exist. Furthermore, similar to the results found for Ni–Al₂O₃ and Cu–Al₂O₃ interfaces containing a film, the Hamaker constant is significantly larger than for a film at a grain boundary in alumina, and as such, films at Au–Al₂O₃ interfaces are expected to be thinner than at grain boundaries in alumina [30–32].

Following Clarke's model, a surface film can exist on sapphire if the refractive index of the film is larger than 1.72 using an UV absorption frequency of $3.5\cdot10^{15}$ Hz (see Fig. 14). Below this value the Hamaker constant will be negative, indicating that the film is not stable. Assuming this explanation is correct, it necessarily means that the concentration of

Table 3 Data used to calculate the Hamaker constant

	$\upsilon_{\text{e,ceramic}}$[1/s]	Refractive index	$\varepsilon_{(0)}$	Reference
Al₂O₃	3.18×10^{15}	1.753	10.1	[61]
SiO₂ [Fused Silica]	3.24×10^{15}	1.448	3.82	[61]
Au	$\upsilon_{\text{e,metal}}$[1/s]			
	6.2×10^{15}			[62]

Table 4 Refractive indices of different compositions in the SiO₂–Al₂O₃–CaO ternary system (crystalline phases) [63]

Notation	Formula	Refractive Index
Anorthite	CaO–Al₂O₃–2SiO₂	1.572–1.588
Cristobalite	SiO₂	1.486
Corundum	Al₂O₃	1.764
Gehlenite	2CaO–Al₂O₃–SiO₂	1.665
Lime	CaO	1.838
Mullite	3Al₂O₃–2SiO₂	1.642–1.679
Rankinite	3CaO–2SiO₂	1.64–1.65

the surface film detected on sapphire has a composition significantly different than that of the film at the Au–Al_2O_3 interface. The composition and Hamaker constant of the film at the Au–Al_2O_3 interfaces, and the film on the surface of the sapphire, remain to be characterized, and will be the focus of a future study [64].

The purpose of these calculations was to demonstrate that a film can theoretically exist at Au-sapphire interfaces, and that for certain compositions (and thus above certain values of the refractive index), a surface film on sapphire is expected to be stable. A force-balance calculation was not made, since this depends on a number of unknown factors, including the degree of structural order within the film. While determining the degree of order in the film is beyond the scope of this article, it is expected to influence the repulsive force, and hence the force balance and the expected stabilized film thickness [32, 48, 49, 65]. The issue of structural order in the film has been addressed in a number of experimental [23, 28] and computational studies [24, 25].

Summary and conclusions

The existence of nanometer-thick amorphous equilibrium films at metal-ceramic interfaces has been experimentally verified for the Au–Al_2O_3 system. This revokes previous speculation regarding creation of the film due to oxidation of the metal (which might be possible at Cu–Al_2O_3 and Ni–Al_2O_3 interfaces). HRTEM micrographs of the interface with and without the presence of anorthite, in addition to qualitative analytical TEM, validated the existence of the film. The thickness of the films (~1 nm) was measured from HRTEM micrographs, which is comparable to values found for films at Ni–Al_2O_3 and Cu–Al_2O_3 interfaces. In addition, HRTEM investigations showed the existence of a ~1 nm thick film on the surface of (0001) sapphire which was partially wetted with anorthite drops.

The Hamaker constant was calculated for the Au-film-Al_2O_3 interface, which confirmed that an attractive van der Waals force can exist at this interface. From the Hamaker calculations it has been shown that for certain compositions a surface film may exist on the surface of sapphire.

References

1. Clarke DR, Thomas G (1977) J Am Ceram Soc 60: 491
2. Clarke DR, Thomas G (1978) J Am Ceram Soc 61: 114
3. Clarke DR (1979) Ultramicroscopy 4: 33
4. Falk LKL (1997) J Eur Ceram Soc 17: 983
5. Falk LKL (1998) J Eur Ceram Soc 18: 2263
6. Nagano T, Kaneko K, Zhan G-D, Mitomo M (2000) J Am Ceram Soc 83: 2781
7. Volz E, Roosen A, Wang S-C, Wei W-CJ (2004) J Mater Sci 39: 4095
8. Lee J-H, Kim D-Y, Kim Y-W (2006) J Eur Ceram Soc 26: 1267
9. Zhang XF, Sixta ME, Jonghe LC (2000) J Am Ceram Soc 83: 2813
10. Brydson R, Chen S-C, Riley FL, Milne SJ, Pan X, Ruhle M (1998) J Am Ceram Soc 81: 369
11. Swiatnicki W, Lartigue-Korinek S, Laval JY (1995) Acta Metall Mater 43: 795
12. Brydson R, Twigg PC, Loughran F, Riley FL (2001) J Mater Res 16: 652
13. Chiang Y-M, Silverman LA, French RH, Cannon RM (1994) J Am Ceram Soc 77: 1143
14. Wang H, Chiang Y-M (1998) J Am Ceram Soc 81: 89
15. Luo J, Wang H, Chiang Y-M (1999) J Am Ceram Soc 82: 916
16. Luo J, Chiang Y-M (2000) Acta Mater 48: 4501
17. Kleebe H-J, Cinibulk MK, Cannon RM, Ruhle M (1993) J Am Ceram Soc 76: 1969
18. Tanaka I, Kleebe H-J, Cinibulk MK, Bruley J, Clarke DR, Ruhle M (1994) J Am Ceram Soc 77: 911
19. Gu H, Pan X, Cannon RM, Ruhle M (1998) J Am Ceram Soc 81: 3125
20. French RH, Mullejans H, Jones DJ, Duscher G, Cannon RM, Ruhle M (1998) Acta Mater 46: 2271
21. Becher PF, Painter GS, Sun EY, Hsueh CH, Lance MJ (2000) Acta Mater 48: 4493
22. Yoshiya M, Tanaka I, Adachi H (2000) Acta Mater 48: 4641
23. Shibata N, Pennycook SJ, Gosnell TR, Painter GS, Shelton WA, Becher PF (2004) Nature 428: 730
24. Su XT, Garofalini SH (2004) J Mater Res 19: 3679
25. Su X, Garofalini SH (2004) J Mater Res 19: 752
26. Rulis P, Chen J, Ouyang L, Ching WY, Su X, Garofalini SH (2005) Phys Rev B 71: 235317/1
27. Su X, Garofalini SH (2005) J Appl Phys 97: 113526/1
28. Winkelman GB, Dwyer C, Hudson TS, Nguyen-Manh D, Doblinger M, Satet RL, Hoffmann MJ, Cockayne DJH (2005) Appl Phys Lett 87: 061911
29. Scheu C, Dehm G, Kaplan WD (2001) J Am Ceram Soc 84: 623
30. Avishai A, Scheu C, Kaplan WD (2003) Z Metallkd 94: 272
31. Avishai A, Scheu C, Kaplan WD (2005) Acta Mater 53: 1559
32. Avishai A, Kaplan WD (2005) Acta Mater 53: 1571
33. Kleebe H-J, Hoffmann MJ, Ruehle M (1992) Z Metallkd/ Mater Res Adv Tech 83: 610
34. Knowles KM, Turan S (2000) Ultramicroscopy 83: 245
35. Powell-Dogan CA, Heuer AH, Ready MJ, Merriam K (1991) J Am Ceram Soc 74: 646
36. Jin Q, Wilkinson DS, Weatherly GC (1999) J Am Ceram Soc 82: 1492
37. Becher PF, Sun EY, Plucknett KP, Alexander KB, Hsueh C-H, Lin H-T, Waters SB, Westmoreland CG, Kang E-S, Hirao K, Brito ME (1998) J Am Ceram Soc 81: 2821
38. Sun EY, Becher PF, Plucknett KP, Hsueh C-H, Alexander KB, Waters SB, Hirao K, Brito ME (1998) J Am Ceram Soc 81: 2831

39. Padture NP (1994) J Am Ceram Soc 77:519
40. Sun EY, Becher PF, Hsueh C-H, Painter GS, Waters SB, Hwang S-L, Hoffmann MJ (1999) Acta Mater 47: 2777
41. Chen D, Sixta ME, Zhang XF, De Jonghe LC, Ritchie RO (2000) Acta Mater 48: 4599
42. Moberlychan WJ, De Jonghe LC (1998) Acta Mater 46: 2471
43. Chen, Zhang X-F, Ritchie RO (2000) J Am Ceram Soc 83: 2079
44. De Graef M, Dalgleish BJ, Turner MR, Evans AG, Acta Metall Mater 40 (1992)
45. Pandit R, Schick M, Wortis M (1982) Phys Rev B 26: 5112
46. Cahn JW (1977) J Chem Phys 66: 3667
47. Cannon RMR, Hoffmann MJ, French RH, Gu H, Tomsia AP, Saiz E (2000) In: Sakuma T, Sheppard LM, Ikuhara Y (eds) Grain boundary engineering in ceramics, American Ceramic Society, p 427
48. Clarke DR (1987) J Am Ceram Soc 70: 15
49. Clarke DR, Shaw TM, Philipse AP, Horn RG (1993) J Am Ceram Soc 76: 1201
50. Chatain D, Chabert F, Ghetta V, Fouletier J (1993) J Am Ceram Soc 76: 1568
51. Sugiyama M, Sigesato G (2004) J Electron Microsc 53: 527
52. Ando M, Katoh Y, Tanigawa H, Kohyama A (1999) J Nucl Mater 271–272: 111
53. Sadan H, Kaplan WD (2006) J Mater Sci 41: 5099
54. Heffelfinger JR, Bench MW, Carter CB (1997) Surf Sci 370: L168
55. Ravishankar N, Carter CB (2000) Int Sci 8: 295
56. Ravishankar N, Gilliss SR, Carter CB (2003) J Eur Ceram Soc 23: 2777
57. Saiz E, Tomsia AP, Cannon RM (1998) Acta Mater 46: 2349
58. Levi G, Kaplan WD (2002) Acta Mater 50: 75
59. Levi G, Kaplan WD (2003) Acta Mater 51: 2793
60. Oh SH, Kauffmann Y, Scheu C, Kaplan WD, Ruhle M (2005) Science 310: 661
61. Bergstrom L (1997) Adv Colloid Interfac 70: 125
62. Lipkin DM, Clarke DR, Evans AG (1998) Acta Mater 46: 4835
63. http://www.webmineral.com/data/, as on 31 March 2006
64. French RH (2000) J Am Ceram Soc 83: 2117
65. Kaplan WD, Kauffmann Y (2006) Ann Rev Mater Res 36: 1